Environmental Science Nano

ROYAL SOCIETY OF CHEMISTRY

PAPER

View Article Online
View Journal | View Issue

Check for updates

Cite this: *Environ. Sci.: Nano*, 2025, **12**, 2799

About the effects of true-to-life polyethylene terephthalate nanoparticles on macrophages†

Véronique Collin-Faure,[a] Aliro Villacorta,[bc] Marianne Vitipon,[a] Hélène Diemer,[de] Sarah Cianférani,[de] Ricard Marcos,[b] Elisabeth Darrouzet,[a] Alba Hernandez[b] and Thierry Rabilloud *[a]

Plastics are emerging pollutants of great concern. Macroplastics degrade into microplastics and nanoplastics, which can accumulate in living organisms with still poorly known consequences. Nanoplastics being particulate pollutants, they are handled in animal organisms by scavenger cells such as macrophages, which are important players in the immune system. Polyethylene terephthalate is one of these plastics of concern, as it is widely used in food packaging where it releases nanoparticles. We have thus undertaken a study on the effects of true-to-life polyethylene terephthalate nanoparticles prepared from water bottles on macrophages. To this purpose, we used a combination of proteomics and targeted validation experiments. Proteomics showed important adaptive changes in the proteome in response to exposure to polyethylene terephthalate nanoparticles. These changes affected not only mitochondrial, cytoskeletal and lysosomal proteins, for example, but also proteins implicated in immune functions. Validation experiments showed that many of these changes were homeostatic, with no induced oxidative stress and no gross perturbation of the mitochondrial function. However, polyethylene terephthalate nanoparticles induced endoplasmic reticulum stress and disturbed the immune functions of macrophages. We indeed observed a slight pro-inflammatory response (1.5-fold increase in TNF secretion). We also observed a decrease in the response to bacterial stimulation (1.6-fold decrease in IL-6 secretion). We also observed a 20% decrease in the expression of important proteins involved in immune responses such as TLR2, TLR7 or collectin 12, and a twofold decrease in the production of lysozyme. This suggests that macrophages having ingested polyethylene terephthalate nanoparticles are less efficient in their immune functions.

Received 13th November 2024,
Accepted 28th March 2025

DOI: 10.1039/d4en01063a

rsc.li/es-nano

Open Access Article. Published on 01 April 2025. Downloaded on 2/6/2026 8:59:39 AM.
This article is licensed under a Creative Commons Attribution-NonCommercial 3.0 Unported Licence.

Environmental significance

Plastic pollution is a concerning topic, *e.g.* because of the degradation of plastics in nanoparticles that are easily uptaken by living organisms and poorly degradable. It is therefore necessary to investigate in detail the effects of plastic particles on living cells. However, this shall be best made on particles obtained from real plastic objects (true-to-life nanoplastics). Consequently, we have studied the effects of polyethylene terephthalate nanoparticles on macrophages, *i.e.* professional phagocytes conserved in evolution, by a combination of proteomic and targeted approaches. Plastics-exposed cells showed on the one hand a slight pro-inflammatory response and on the other hand a decreased ability to respond to a bacterial stimulus, suggesting slightly impaired immune functions of macrophages after exposure to plastics.

1. Introduction

The wide use of plastics in very diverse areas (*e.g.* packaging, automotive, textile, and electronics, to quote just a few) translates into a tremendous production, *i.e.* close to a gigaton per year.[1] Unfortunately, almost half of this tonnage is released yearly in the environment,[2] where it has deleterious effects that are more and more documented in detail, *e.g.* on seabirds,[3] but also on many other marine taxa.[4] This is due to the fact that this pollution was first documented in aquatic marine environments,[5–8] but it has now been found in many other environments, ranging from

[a] *Chemistry and Biology of Metals, CNRS UMR5249, CEA, IRIG-LCBM, Univ. Grenoble Alpes, F-38054 Grenoble, France. E-mail: thierry.rabilloud@cnrs.fr*
[b] *Group of Mutagenesis, Department of Genetics and Microbiology, Faculty of Biosciences, Universitat Autònoma de Barcelona, Cerdanyola del Vallès, Barcelona, Spain*
[c] *Facultad de Recursos Naturales Renovables, Universidad Arturo Prat, Iquique, Chile*
[d] *Laboratoire de Spectrométrie de Masse BioOrganique (LSMBO), IPHC UMR 7178, CNRS, Université de Strasbourg, 67087 Strasbourg, France*
[e] *Infrastructure Nationale de Protéomique ProFI – UAR 2048, 67087 Strasbourg, France*

† Electronic supplementary information (ESI) available. See DOI: https://doi.org/10.1039/d4en01063a

Open Access Article. Published on 01 April 2025. Downloaded on 2/6/2026 8:59:39 AM. This article is licensed under a Creative Commons Attribution-NonCommercial 3.0 Unported Licence.

marine sediments[9,10] to freshwater[11–13] and terrestrial environments.[14,15]

Although plastics are often used for their chemical and mechanical resistance, resulting in half-lives amounting to decades in the natural environments,[16] they fragment over time, first into microplastics (lesser than 5 mm in size) and then into nanoplastics (less than 1 μm in size). These nanoplastics are far more difficult to detect in the environment, and their effects are much less known. It is however predicted that the smaller the nanoplastic particles, the easier they will cross the biological barriers, resulting in putative deleterious effects on living organisms.

This hypothesis has prompted extensive research on the effects of micro- and nanoplastics on a wide variety of living organisms from various phyla, ranging from worms[17,18] to mollusks,[19,20] crustaceans,[21,22] insects,[23,24] and then vertebrates such as fish[25–27] and of course mammals[28,29] including human models (*e.g.* in ref. 29–33). However, a significant part of this research has been carried out with model and controlled pristine spherical nanoparticles, most often polystyrene because of its facility of production in a wide range of controlled sizes. Polystyrene is indeed well represented in plastic wastes,[6,8] which renders such research relevant for investigating the core effects of the polymer by itself and also for investigating the effects of parameters such as particle size.[34,35] However, such synthetic spherical particles cannot fully represent the effects of environmentally found particles, so that such studies must be extended to other types of plastics that can be obtained as non-spherical particles and that are well represented in plastic waste. Within this frame, an interesting approach is represented by particles obtained from plastic objects by various mechanical and chemical processes, which represent true-to-life nanoplastics.

Polyethylene terephthalate (PET) represents one case of plastics that is amenable to the production of such true-to-life nanoparticles.[36,37] It also represents an environmentally relevant plastic, as PET is widely used for packaging of liquids and in the textile industry. Indeed, recent studies have shown that PET bottles do release nanoparticles under standard conditions of use.[38–40] It is thus highly relevant to investigate the effects of true-to life PET particles on living cells, and the cell types of interest are dictated by each organism's physiology. We define as a true-to-life NPL those plastic nanoparticles obtained from the degradation of plastic goods under laboratory conditions. Thus, the degradation of PET water plastic bottles (as an example) can produce true-to-life PET NPLs.[37]

Multicellular organisms defend themselves against particles, including plastic particles, by a series of mechanisms. The first line of defense is represented by biological barriers (*e.g.* intestinal[29] or epidermal barriers) and research has been devoted to understanding how these barriers interact with plastic particles. When translocation across these barriers occurs,[29] then a second line of barriers comes into play and is represented by professional phagocytes. This cell type is encountered in invertebrates (annelid coelomocytes, insect hemocytes) as well as in vertebrates (macrophages, neutrophils). Indeed, it has been shown that this cell type responds strongly to plastic particles.[18,24,34,35,41–43]

aWe thus decided to investigate the responses of macrophages to PET nanoparticles using a combination of proteomic and targeted approaches, as previously done with polystyrene (PS)[34] and polylactide (PLA)[44] nanoparticles.

2. Materials and methods

2.1. True-to-life PET NPL obtention and characterization

PET NPLs were obtained following a previously published protocol.[37] Briefly, starting from commercially available polyethylene terephthalate bottles, nanoparticles were produced by sanding the material with a diamond rotary burr. The resulting powder underwent multiple processing steps, as outlined in Fig. 1a. Briefly, the sanded powder was sieved through a 0.20 mm mesh, and 4 g of the sieved material were placed in a 250 mL beaker containing 60 °C pre-warmed 90% trifluoroacetic acid (TFA) for 2 h or until complete dispersion on a stirring hot plate. The temperature was reduced to 25 °C, and agitation was maintained overnight. On the second day, an equal volume of 20% TFA was carefully added to the mixture and large agglomerates were removed. Finally, after 24 h of stirring, the mixture was transferred to glass tubes and centrifuged for 1 h at 2500 rcf. Pellets were resuspended in 0.5% sodium dodecyl sulfate (SDS) lysis buffer solution and sonicated before transferring to four 250 mL graduated cylinders. The bigger fraction was allowed to settle for 1 h and the top 100 mL of each cylinder was recovered and carefully washed twice with water and pure ethanol. Finally, the material was sonicated and aliquoted to be used in biological experiments. To determine their physicochemical characteristics, a comprehensive characterization of the PET NPLs was conducted using transmission electron microscopy (TEM), nanoparticle tracking analysis (NTA), dynamic light scattering (DLS), and Fourier-transform infrared (FTIR) spectroscopy.

TEM was employed to assess particle size and morphology according to established protocols.[37] Martin diameters were measured on 1000 randomly selected images using ImageJ software version 1.8.0_322. Particle size and concentration in suspension were also analyzed with a Nanosight NS300 particle analyzer (Malvern Panalytical, Cambridge, UK). The suspension behavior was further evaluated by determining particle size distribution through DLS using a Zetasizer® Ultra Red Label apparatus (Malvern Panalytical, Cambridge, UK). DLS values were determined in water and cell culture (DMEM) medium. Finally, FTIR analysis was performed to identify functional groups in the PET NPLs, with the obtained spectra compared to standard references. All characterization methods are comprehensively detailed in ref. 37.

For some experiments, the PET particles were labelled with the deep fluorescent red Disperse Blue 14 (1,4-bis(methylamino) anthraquinone, ABCR #AB177338, λ_{ex} 640 nm, λ_{em} 685 nm) by the solvent swelling method.[45] Briefly, a 10 mg ml^{-1} solution of Disperse Blue 14 in THF was prepared. 1% in volume of this

 This journal is © The Royal Society of Chemistry 2025

Open Access Article. Published on 01 April 2025. Downloaded on 2/6/2026 8:59:39 AM.
This article is licensed under a Creative Commons Attribution-NonCommercial 3.0 Unported Licence.

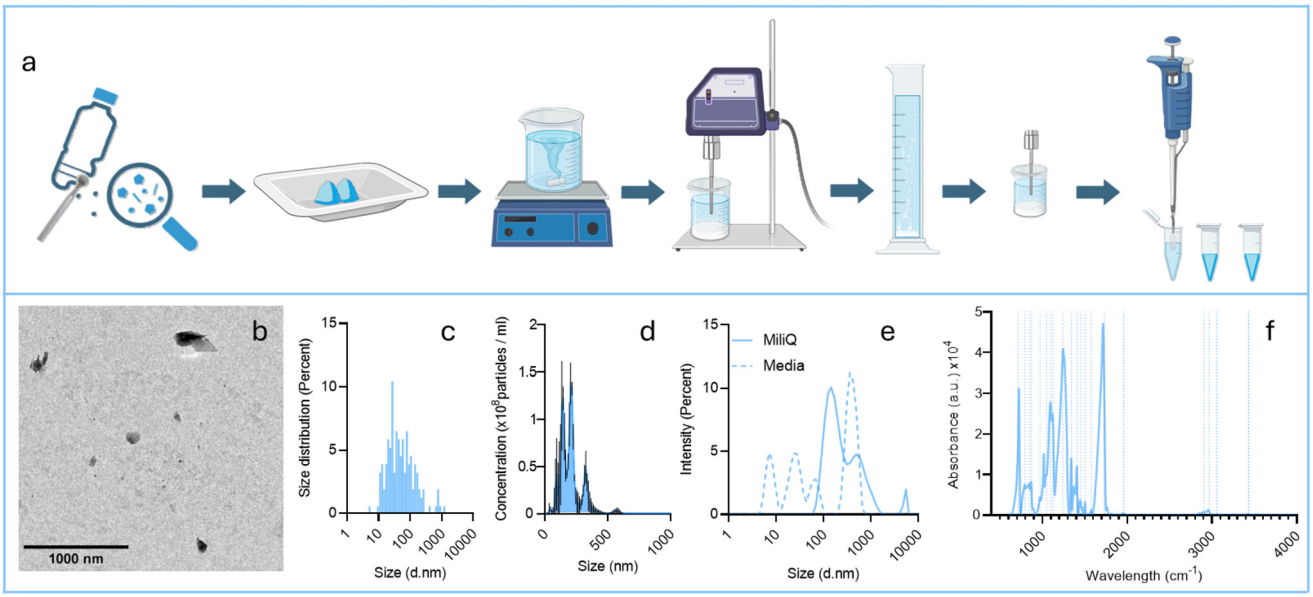

Fig. 1 Schematic presentation of the method used to obtain PET NPs (a). TEM image (b) and its size distribution (c). Size distribution was also determined by nanotracking analysis (NTA) (d) and dynamic light scattering (DLS) (e). Finally, the chemical identity of functional groups was confirmed by Fourier-transform infrared (FTIR) spectroscopy (f). The size determined by NTA was 205.6 ± 7.7 nm, while the sizes determined by DLS were 292 ± 26 nm (in water) and 362 ± 16 (in DMEM), with polydispersity indexes of 0.47 and 0.54, respectively.

solution was added to the PET nanoparticle suspension, and the mixture was agitated on a rotary wheel at room temperature for 30 minutes. Two volumes of water were then added and the particles were collected by centrifugation (30 minutes at 15 000*g*). The pellet was then resuspended in water and the beads recollected by centrifugation. The final pellet was then resuspended in 20% ethanol for sterilization for 1 h, then centrifuged as described above and finally resuspended in sterile ultrapure water. To measure fluorophore leakage, a 80 μg ml^{-1} of fluorescently-labelled particles was prepared in phenol red-free DMEM supplemented with 10% fetal bovine serum, and its fluorescence measured using a DeNovix QFX fluorimeter (excitation 635 nm, emission 665–740 nm). The suspension was then incubated for 24 h at 37 °C. At the end of the incubation period, the suspension was centrifuged (30 minutes at 15 000*g*), the supernatant was removed, the particle pellet was resuspended in the initial volume of phenol red-free DMEM supplemented with 10% fetal bovine serum and its fluorescence was read again using the same parameters.

2.2. Cell culture

The J774A.1 cell line (mouse macrophages) was purchased from European Cell Culture Collection (Salisbury, UK). Cells were routinely propagated in DMEM supplemented with 10% fetal bovine serum (FBS) in non-adherent flasks (Cellstar flasks for suspension culture, Greiner Bio One, Les Ulis, France). For routine culture, the cells were seeded at 200 000 cells per ml and passaged two days later, with a cell density ranging from 800 000 to 1 000 000 cells per ml. For exposure to plastic particles and to limit the effects of cell growth, cells were seeded at 500 000 cells per ml in 6 or 12 well plates, allowed to settle and recover for 24 h, and then exposed to the particles at 50 μg ml^{-1} for 24 h before harvesting for the experiments. Proteomic experiments were carried out in 6 well plates, and all the other experiments in 12 well plates. The medium volume was adjusted to keep the same height across all cell culture formats. Cells were used at passage numbers from 5 to 15 post-reception from the repository. Cell viability was measured by the propidium iodide method[46] or with a SYTOX Green probe (Thermo Fisher, S7020) using the protocol provided by the supplier.

In order to measure the particles' internalization, cells were treated in 12 well plates (1 ml culture medium volume) for 24 h with 50 μg ml^{-1} fluorescently labelled polystyrene (250 nm nominal diameter, Spherotech #FP-0270-2) or PET nanoparticles as well as with fluorescently labelled PLA beads (150 nm nominal diameter, Adjuvatis #RFIP-600-150) for comparison. At the end of the incubation period, the culture medium was removed and the cell layer was rinsed with PBS. The cell layer was then lysed in 500 μl of 10 mM HEPES pH 7.5, and the lysate fluorescence was measured using a DeNovix QFX fluorimeter (Exc 635 nm, Em 665–740 nm). In order to compare this fluorescence with the initial input, 50 μg of the particles were suspended in 500 μl of 10 mM HEPES pH 7.5 and the fluorescence was measured as for the cell lysates.

In order to obtain further insights on the PET NPL internalization, J774 cells were first treated for 1 h with inhibitors (12.5–25 μg ml^{-1} nystatin[47] or 100–200 μM dimethylamiloride[48] or 20–30 μM trifluoperazin[49]). Fluorescent PET NPLs were then added at a concentration of 5 μg ml^{-1} and the cells were allowed to internalize the particles for 3 h. At the end of this incubation period, the culture medium was

Open Access Article. Published on 01 April 2025. Downloaded on 2/6/2026 8:59:39 AM. This article is licensed under a Creative Commons Attribution-NonCommercial 3.0 Unported Licence.

removed, the cells were harvested in cold culture medium, rinsed once by centrifugation and their fluorescence measured by flow cytometry (Exc 635 nm, Em 670–750 nm). As a control, yellow-green fluorescently labelled 1 μm polystyrene beads (Polysciences #15702-10) were used (Exc 488 nm, Em 540 nm).

2.3. Proteomics

Proteomics was carried out essentially as described previously.[34] However, the experimental details are given here for the sake of consistency.

2.3.1. Sample preparation. After exposure to the plastic particles, the cells were harvested by flushing the 6 well plates. They were collected by centrifugation (200*g*, 5 minutes) and rinsed twice in PBS. The cell pellets were lysed in 100 μl of extraction buffer (4 M urea, 2.5% cetyltrimethylammonium chloride, 100 mM sodium phosphate buffer pH 3, 150 μM methylene blue). The extraction was allowed to proceed at room temperature for 30 minutes, after which the lysate was centrifuged (15 000*g*, 15 minutes) to pellet the nucleic acids. The supernatants were then stored at −20 °C until use.

2.3.2. Shotgun proteomics. For the shotgun proteomic analysis, the samples were included in polyacrylamide plugs according to Muller *et al.*,[50] with some modifications to downscale the process.[51] For this purpose, a photopolymerization system using methylene blue, toluene sulfinate and diphenyliodonium chloride was used.[52]

As mentioned above, methylene blue was included in the cell lysis buffer. The other initiator solutions consisted of a 1 M solution of sodium toluene sulfinate in water and in a saturated water solution of diphenyliodonium chloride. The ready-to-use polyacrylamide solution consisted of 1.2 ml of a commercial 40% acrylamide/bis solution (37.5/1) to which 100 μl of diphenyliodonium chloride solution, 100 μl of sodium toluene sulfinate solution and 300 μl of water were added.

To the protein samples (15 μl), 5 μl of acrylamide solution were added and mixed by pipetting in a 500 μl conical polypropylene microtube. 100 μl of water-saturated butanol were then layered on top of the samples, and polymerization was carried out under a 1500 lumen 2700 K LED lamp for 2 h, during which the initially blue gel solution discolored. At the end of the polymerization period, the butanol was removed, and the gel plugs were fixed for 1 h with 200 μl of 30% ethanol and 2% phosphoric acid, followed by 3× 15 minute washes in 20% ethanol. The fixed gel plugs were then stored at −20 °C until use.

Gel plug processing, digestion, peptide extraction and nanoLC-MS/MS were performed as previously described,[51] without the robotic protein handling system and using a Q-Exactive Plus mass spectrometer (Thermo Fisher Scientific, Bremen, Germany). Further details are available in Methods S1.†

For protein identification, the MS/MS data were interpreted using a local Mascot server with MASCOT 2.6.2 algorithm (Matrix Science, London, UK) against an in-house database containing all *Mus musculus* and *Rattus norvegicus* entries from UniProtKB/SwissProt (version 2019_10, 25156 sequences) and the corresponding 25156 reverse entries. Spectra were searched with a mass tolerance of 10 ppm for MS and 0.05 Da for MS/MS data, allowing a maximum of one trypsin missed cleavage. Trypsin was specified as the enzyme. Acetylation of protein N-termini, carbamidomethylation of cysteine residues and oxidation of methionine residues were specified as variable modifications. Identification results were imported into Proline software version 2.2 (**https://profiproteomics.fr/proline**) for validation. Peptide spectrum matches (PSM) with pretty rank equal to one and a length greater than 7 amino acids were retained. The false discovery rate (FDR) was then optimized to be below 1% at PSM level using Mascot adjusted *E*-value and below 1% at protein level using Mascot Standard score.

Mass spectrometry data are available *via* ProteomeXchange with the identifier PXD062730.

2.3.3. Label free quantification. Peptide abundances were extracted thanks to Proline software version 2.2 (**https://profiproteomics.fr/proline**) using a *m*/*z* tolerance of 10 ppm. Alignment of the LC-MS runs was performed using Loess smoothing. Cross assignment was performed within groups only. Protein abundances were computed by the sum of peptide abundances (normalized using the median).

2.3.4. Data analysis. For the global analysis of the protein abundance data, missing data were imputed with a low, non-null value. Proteins that were detected less than 3 times out of 5 in both groups were removed from the analysis. The complete abundance dataset was then analyzed using PAST software.[53]

Proteins were considered as significantly different if their *p* value in the Mann–Whitney *U*-test against control values was less than 0.05. No quantitative change threshold value was applied. The selected proteins were then submitted to pathway analysis using the DAVID tool[54] with a cutoff value set at a FDR of 0.25.

2.4. Mitochondrial transmembrane potential assay

The mitochondrial transmembrane potential assay was performed essentially as described previously.[35] Rhodamine 123 (Rh123) was added to the cultures at an 80 nM final concentration (to avoid quenching[55]), and the cultures were further incubated at 37 °C for 30 minutes. At the end of this period, the cells were collected, washed in cold PBS containing 0.1% glucose, resuspended in PBS glucose and analyzed for the green fluorescence (excitation 488 nm emission 525 nm) on a Melody flow cytometer. As a positive control, butanedione monoxime (BDM) was added at a 30 mM final concentration together with the Rh123.[56] As a negative control, carbonyl cyanide 4-(trifluoromethoxy)phenylhydrazone (FCCP) was added at 5 μM final concentration together with the Rh123.[56]

2.5. Lysosomal assay

For the lysosomal function assay, the Lysosensor method was used as described previously.[35] After exposure to plastic particles, the medium was removed, the cell layer was rinsed

 This journal is © The Royal Society of Chemistry 2025

Open Access Article. Published on 01 April 2025. Downloaded on 2/6/2026 8:59:39 AM. This article is licensed under a Creative Commons Attribution-NonCommercial 3.0 Unported Licence.

with complete culture medium and incubated with 1 μM Lysosensor Green (Molecular Probes) diluted in warm (37 °C) complete culture medium for 1 h at 37 °C. At the end of this period, the cells were collected, washed in cold PBS containing 0.1% glucose, resuspended in PBS glucose and analyzed for the green fluorescence (excitation 488 nm emission 540 nm) on a Melody flow cytometer.

2.6. Assay for oxidative stress

For the oxidative stress assay, a protocol based on the oxidation of dihydrorhodamine 123 (DHR123) was used, essentially as described previously.[35] After exposure to plastic particles, the cells were treated in PBS containing 500 ng ml^{-1} DHR123 for 20 minutes at 37 °C. The cells were then harvested, washed in cold PBS containing 0.1% glucose, resuspended in PBS glucose and analyzed for green fluorescence (same parameters as for rhodamine 123) on a Melody flow cytometer. Menadione (applied on the cells for 2 h prior to treatment with DHR123) was used as a positive control in a concentration range of 25–50 μM.

2.7. Phagocytosis assay

For this assay,[57] the cells were first exposed to PET particles. After 24 h of exposure, the cells were then exposed to 0.5 μm latex beads (carboxylated surface, yellow green-labelled, from Polysciences, excitation 488 nm, emission 527/32 nm) for 3 h. After this second exposure, the cells were collected, rinsed once with PBS, and analyzed for the two fluorescences (green and red) on a Melody flow cytometer.

2.8. Cytokine release assays

Cells were first exposed to nanoplastics (50 μg ml^{-1}) for 24 h. At the end of this exposure period, the culture medium was removed, the cell layer was rinsed with culture medium and fresh medium was added to the wells. In half of the wells LPS (1 ng ml^{-1}) was added. After another 24 h, the medium was collected and analyzed for proinflammatory cytokines. Tumor necrosis factor (catalog number 558299, BD Biosciences, Le Pont-de-Claix, France) and interleukin 6 (IL-6) (catalog number 558301, BD Biosciences, Le Pont-de-Claix) levels were measured using a Cytometric Bead Array Mouse Inflammation Kit (catalog number 558266, BD Biosciences, Le Pont-de-Claix) and analyzed with FCAP Array software (3.0, BD Biosciences) according to the manufacturer's instructions.

2.9. Cell surface markers

Cells were seeded into 12-well plates at a concentration of 500 000 cells per ml and exposed to plastic particles as described above. For some experiments, LPS was then added at a concentration of 1 ng ml^{-1} 6 h after the exposure to plastic particles. The following day, the cells were harvested and washed in DMEM containing 3% FBS. The cells were then treated with fluorochrome-conjugated antibodies at the adequate dilution for 30 minutes on ice in DMEM–FBS in a final volume of 100 μl. The cells were then washed with 2 ml of PBS. The cell pellet was taken in 400 μl of PBS containing 1 μM Sytox blue for checking cell viability, and the suspension was analyzed by flow cytometry on a Melody flow cytometer. First, live cells (Sytox blue-negative) were selected at 450 nm (excitation at 405 nm). The gated cells were then analyzed for particle fluorescence (excitation 561 nm, emission 695 nm) and for antibody fluorescence (excitation 488 nm, emission 527 nm for FITC- or A488-labelled antibodies or excitation 561 nm, emission 582 nm for PE-conjugated antibodies). Isotypic control antibodies were used to compensate for non-specific binding.

The following antibodies were used:
Collectin-12 (Invitrogen #PA5-47456) dilution 1/6
CD74-FITC (BD-Pharmingen #561-941) dilution 1/25
CD86-FITC (BD-Pharmingen #553-691) dilution 1/50
PD-L1-A488 (BD-Pharmingen #566-864) dilution 1/100
TLR2-FITC (Invitrogen# 11-9021-82) dilution 1/25
TLR7-PE ((BD-Pharmingen #565-557) dilution 1/50

In some experiments with TLR2 and TLR7, the cells were collected after exposure to the plastic particles, washed with PBS, and then fixed and permeabilized using a BD Cytofix-Cytoperm kit (#554715). The cells were incubated with anti-TLR2 or anti-TLR7 antibody diluted to 1/25 or 1/50, respectively, for 30 minutes on ice. The cells were then washed with permeabilization buffer, resuspended in PBS and analyzed by flow cytometry as described above.

3. Results

3.1. PET NPL characterization

True-to-life MNPLs, specifically the PET NPs produced for this study, are not standardized materials. Therefore, accurate characterization of their physicochemical properties is essential. The results of this characterization are summarized in Fig. 1.

The main features of their synthesis are illustrated in Fig. 1a. TEM images (Fig. 1b) reveal that PET NPs exhibit a near-spherical shape with an average diameter of approximately 200 nm. As expected, size variations are observed depending on the methodological approach used (TEM, NTA, and DLS); however, in all cases, the distribution is relatively narrow, predominantly within the 200–300 nm range (Fig. 1c–e). These findings validate the reliability of the protocol employed. To confirm the chemical identity of the PET NPL samples, FTIR analysis was conducted (Fig. 1f). The resulting interferograms were analyzed and compared with previously reported characteristic PET bands, with the observed peaks closely aligning with expected values, thus confirming the PET composition of the samples. Finally, the zeta potential of the PET NPLs were determined as −26.00 ± 1.45 and −6.90 ± 1.34 mV when dispersed in water or in culture medium (DMEM), respectively. These values point out a slight tendency to agglomerate in DMEM. Regarding the fluorescently labelled particles, the fluorescence of an 80 μg ml^{-1} suspension was initially 477 ± 19 fluorescence units, and the particles' associated fluorescence was 475 ± 34 after a 24 h

Open Access Article. Published on 01 April 2025. Downloaded on 2/6/2026 8:59:39 AM.
This article is licensed under a Creative Commons Attribution-NonCommercial 3.0 Unported Licence.

incubation in DMEM + serum, which led to a measured leakage lesser than 1%.

3.2. Viability of the plastic-treated cells

First, the toxic effects of the PET NPs on J774A.1 cells were determined after a 24 h exposure. The results, shown in Fig. 2A, demonstrated a very low toxicity of the PET particles, with an LD40 that reached 200 μg ml^{-1} and an LD20 reaching 100 μg ml^{-1}. As we wanted to be consistent with our previous studies, we decided to use a dose of 50 μg ml^{-1}, *i.e.* the dose used for polystyrene and polylactide nanoparticles.[34,44] This dose was non-toxic, with only 10% mortality, but still induced some functional effects. In order to compare the functional effects to those of PS and PLA nanoparticles at an equal input dose, we estimated the proportion of cell-associated particles after 24 h of exposure using fluorescent particles (Fig. 2B). The data showed that PET NPLs were more efficiently internalized (66%) than PS and PLA nanoparticles, whose internalization was similar (*ca.* 50%).

Finally, we tested the effects of three inhibitors on particle internalization using 1 μm polystyrene beads as a control for beads that are internalized only by phagocytosis. The results (Fig. 2C) showed a higher participation of raft-dependent endocytosis and of macropinocytosis in PET particle internalization compared to 1 μm PS beads.

3.3. Analysis of the proteomic results

The shotgun proteomic analysis was able to detect and quantify 2876 proteins (Table S1†). A first global analysis of the complete protein list by principal component analysis showed that the two groups (control and particle-treated) appeared separated on the diagram (Fig. 3), indicating significative changes in the proteome, even if the chosen concentration was quite remote from the toxicity threshold. The fact that the two proteomes were different, from a statistical point of view, was further substantiated by an analysis of similarities,[58] with a moderate *p*-value of 0.09. Compared to the results obtained with PLA nanoparticles,

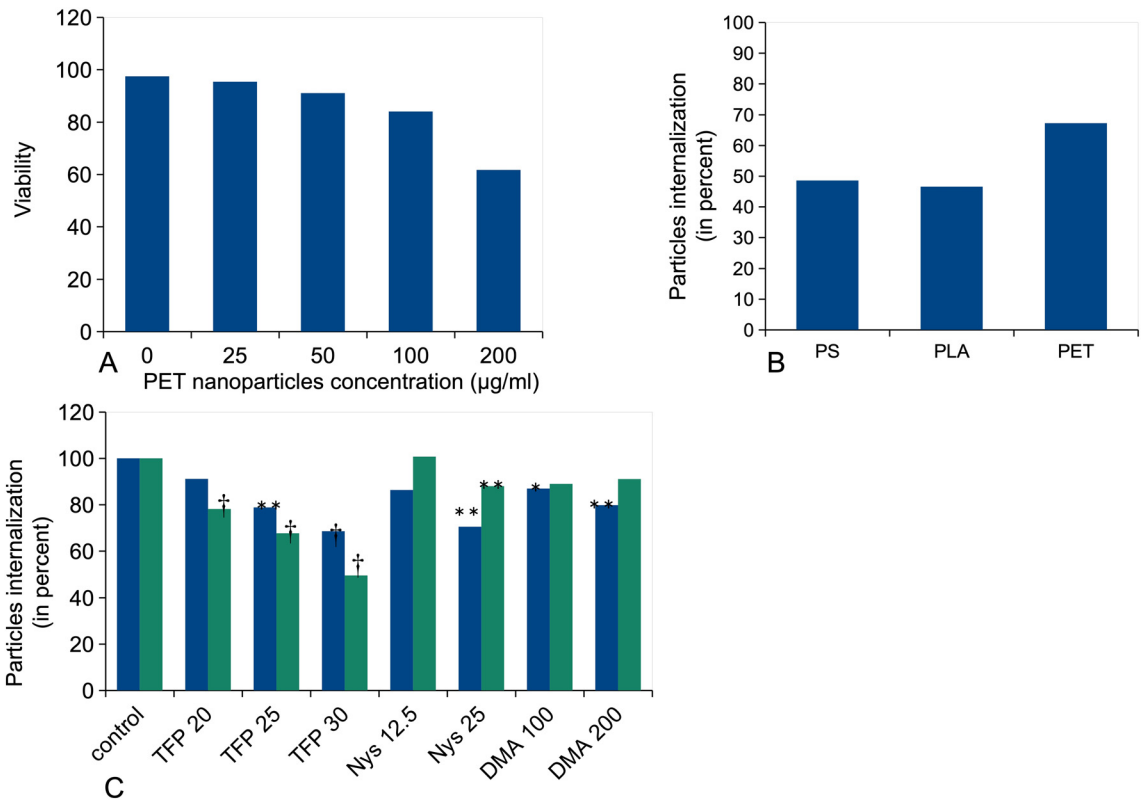

Fig. 2 Viability of cells treated with PET particles; particle internalization. (A) Cells were treated with various concentrations of PET particles for 24 h, and their viability was measured by a flow cytometry fluorophore exclusion assay (Sytox green). Results are displayed as mean ± standard deviation (N = 4). (B) Measurement of relative particle internalization for PET, PS and PLA nanoparticles. Cells were treated with 50 μg ml^{-1} of either blue 14-labelled PET NPLs, sky blue-labelled 200 nm PS nanoparticles or red-labelled 150 nm PLA nanoparticles. The proportion of cell-associated fluorescence after 24 h of exposure compared to input fluorescence is reported. Results are displayed as mean ± standard deviation (N = 4). (C) Influence of endocytosis inhibitors on particle internalization. Cells were first treated with the inhibitors for 1 h, then the particles were added and the incubation was prolonged for 3 h. The cells were then collected and the fluorescence of the internalized particles was measured by flow cytometry. Results are displayed as mean ± standard deviation (N = 4). Blue bars: cells treated with blue 14-labelled PET NPLs. Green bars: cells treated with 1 μm diameter yellow-green labelled polystyrene beads. TFP: trifluoperazine (phagocytosis inhibitor, concentrations expressed in μM). Nys: nystatin (inhibitor of raft-dependent endocytosis, concentrations expressed in μg ml^{-1}). DMA: dimethylamiloride (macropinocytosis inhibitor, concentrations expressed in μM)). Significance symbols (for t-test against the control values): *$p < 0.05$; **$p < 0.01$; †$p < 0.001$.

This journal is © The Royal Society of Chemistry 2025

Open Access Article. Published on 01 April 2025. Downloaded on 2/6/2026 8:59:39 AM.
This article is licensed under a Creative Commons Attribution-NonCommercial 3.0 Unported Licence.

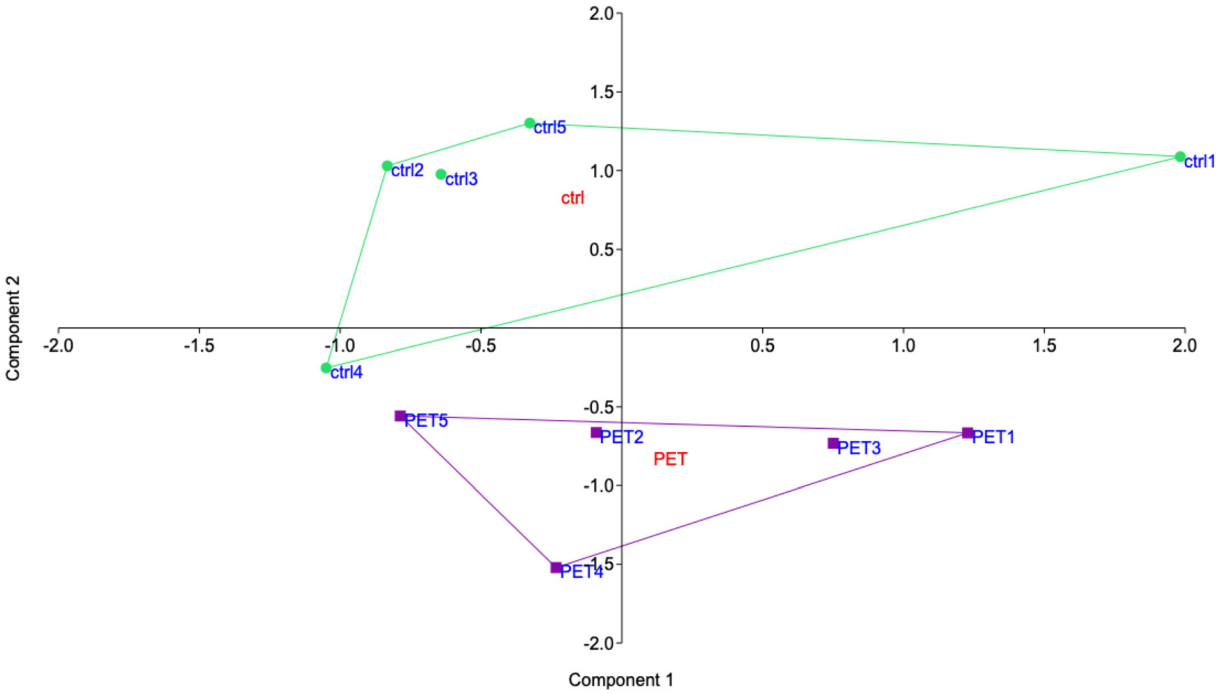

Fig. 3 Global analysis of the proteomic data. The complete proteomic data table (2876 proteins) was analyzed by principal component analysis, using the PAST software. The results are represented as the *X*–*Y* diagram of the first two axes of the principal component analysis, representing 69% of the total variance. Eigenvalue scale.

where the *p*-value was ten times lower, this indicates lesser effects of the PET particles on a proteome-wide scale.

Proteins modulated by the internalization of PET particles were selected on the basis of a Mann–Whitney *U* test ≤2 in the comparison of plastic-treated cells compared to unexposed controls. This resulted in the selection of 232 modulated proteins (Table S2†). In order to gain further insight into the significance of the observed changes, this list of modulated proteins was used to perform pathway analyses by the DAVID software, and the results are shown in Table S3.† Some of the pathways highlighted by this analysis indicated a global stress response (*e.g.* translation, nucleotide binding, endoplasmic reticulum), which is expected for any cellular stress, while other pathways appeared more specific of cellular internalization of particles (*e.g.* mitochondria, lysosomes), and some more related to the macrophages' specialized functions (*e.g.* innate immunity).

3.4. Endoplasmic reticulum and mitochondria

The list of endoplasmic reticulum proteins modulated by cell treatment with PET nanoparticles is presented in Table S4† and included 37 proteins, of which 32 were increased in abundance in response to PET nanoparticles. Many of the proteins detected were involved in lipid biosynthesis and transport (*e.g.* Lss, Mboat7, Elovl1, Osbpl8, Hsd17b12, Acsl5, Atp8a1), a pathway that appears in the DAVID analysis. However, a few proteins were also involved, directly or indirectly, in the ER stress response, such as Retreg1, Ptpn1, Sgpl1, and Canx. This prompted us to test whether ER stress may be involved in PET particles' toxicity. To test this hypothesis we used salubrinal, an inhibitor of the endoplasmic reticulum stress response,[59] which is known to counteract the toxic effects of ER stress on cells.[60] Indeed, as shown in Fig. 4A, salubrinal improved cell survival when cells were treated with high concentrations of PET particles.

A relatively low number of mitochondrial proteins (24) were found modulated in response to PET nanoparticles (Table S5†). Among those, 20 were increased and 4 decreased. We however tested whether these few changes may have a global impact on mitochondria and tested the mitochondrial transmembrane potential. The results, displayed on Fig. 4B, showed no impact of PET internalization on the mitochondrial transmembrane potential, at least at such non-toxic concentrations.

3.5. Lysosomes, oxidative stress, phagocytosis

Only five annotated lysosomal proteins (Atp6v1a, Atp6v1f, Ifi30, M6pr and Pla2g15) were found modulated in response to PET nanoparticles. However, as we had described that treatment of macrophages by PS or PLA nanoparticles increased the lysosomal activity,[44] we decided to check this parameter for PET particles. The results, displayed on Fig. 4C, showed that PET nanoparticles did induce an increase in the lysosomal activity, as the other plastic particles.

In addition to this increased lysosomal activity, we noticed the induction of a mitochondrial protein implicated in the antioxidant response (peroxiredoxin 3 P20108), the induction of a one-electron quinone oxidoreductase (P47199), the

Open Access Article. Published on 01 April 2025. Downloaded on 2/6/2026 8:59:39 AM.
This article is licensed under a Creative Commons Attribution-NonCommercial 3.0 Unported Licence.

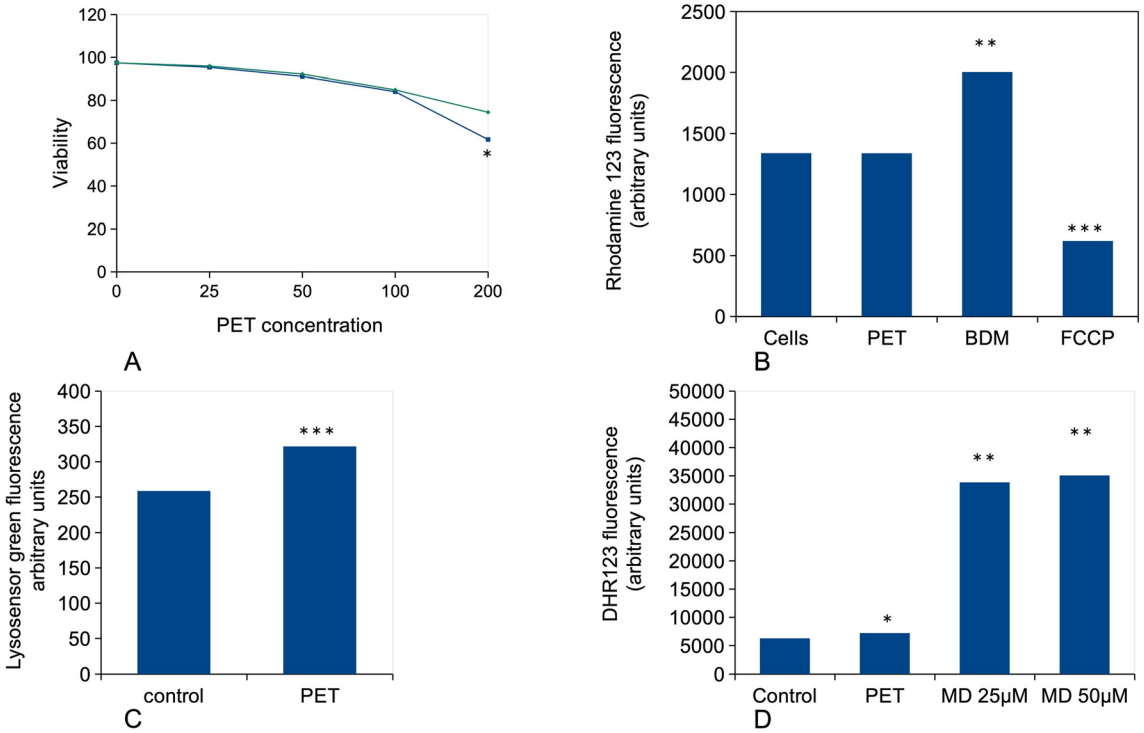

Fig. 4 Mitochondria, lysosomes, oxidative stress and endoplasmic reticulum stress experiments. (B–D) The cells were treated for 24 h with 50 μg ml^{-1} PET particles, then various physiological parameters were tested. (A) Test of the endoplasmic stress response in PET toxicity. Cells were pretreated with 20 μM salubrinal for 4 h, and various concentrations of PET NPLs were then added for a further 18 h in culture. At the end of the experiment, the cell viability was measured. Results are displayed as survival curves, with the standard deviations at each tested point (N = 4). Blue curve: cells untreated with salubrinal. Green curve: salubrinal-treated cells. Significance marks: *$p \leq 0.05$ (Student t-test method). (B) Mitochondrial transmembrane potential (rhodamine 123 method). All cells were positive for rhodamine 123 internalization in mitochondria, and the mean fluorescence is the displayed parameter. Results are displayed as mean ± standard deviation (N = 4). BDM: butanedione monoxime. FCCP: carbonyl cyanide 4-(trifluoromethoxy)phenylhydrazone. Significance marks: ** $p \leq 0.01$; *** p 0.001 (Student t-test method). (C) Lysosomal proton pumping (Lysosensor method). All cells were positive for lysosensor internalization in lysosomes, and the mean fluorescence is the displayed parameter. Results are displayed as mean ± standard deviation (N = 4). Significance marks: ***$p \leq 0.001$ (Student t-test method). (D) Cellular oxidative stress, measured with the dihydrorhodamine 123 (DHR123) indicator. The cells were exposed to PET NPLs for 24 h, and finally for 20 minutes to the DHR123 probe. Menadione (25 or 50 μg ml^{-1} for 2 h) was used as a positive oxidative stress control. Results are displayed as mean ± standard deviation (N = 4). Significance marks: *p 0.05; **$p \leq 0.01$ (Student t-test method). MD: menadione.

induction of cytochrome *b*-245 (Q61093), which is an important component of the superoxide producing NADPH oxidase, and the induction of the Romo1 mitochondrial protein (P60603), which produces ROS. This prompted us to investigate if treatment of macrophages by PET particles may induce oxidative stress. The results, displayed in Fig. 4D, showed a moderate (1.14-fold) but significant increase in the oxidative stress response.

In the same trend, we decided to investigate whether PET particles may alter the phagocytic function of macrophages. This effect has been described for PLA particles but not for PS particles.[44]

The labelled PET particles allowed us to determine that the macrophage population was heterogeneous in its internalization capacity of the PET particles, as the PET particle-associated red fluorescence was distributed along 1.5 orders of magnitude (Fig. 5A). For the global population of the PET-treated cells, we did not detect any global change in the phagocytic activity of macrophages (Fig. 5B). However, when the macrophage population was segmented in three populations based on the internalization of plastic particles, as we previously did for PS particles,[35] we observed that the cells that have internalized the highest amount of PET particles are also those which internalize the highest number of phagocytosis test particles afterwards (Fig. 5B and S1†).

3.6. Immunity-related proteins, inflammation

As this function was not detected through the classical pathway analysis, opposite to what was observed for polystyrene particles, we selected among the list of proteins whose expression was significantly modulated in response to exposure to PET particles proteins that are linked to this crucial macrophage function, on the basis of Uniprot annotations. This resulted in a shortlist of 24 proteins (Table S6†). This process highlighted proteins involved in the complement pathway, such as Cfb, Cfp and C1qa, which were all decreased in PET-treated cells, proteins involved in antigen presentation such as Tap1, Tap2, Erap1 (all increased in PET-treated cells) or Ifi30 (decreased), proteins directly involved in antibacterial defense

 This journal is © The Royal Society of Chemistry 2025

Open Access Article. Published on 01 April 2025. Downloaded on 2/6/2026 8:59:39 AM. This article is licensed under a Creative Commons Attribution-NonCommercial 3.0 Unported Licence.

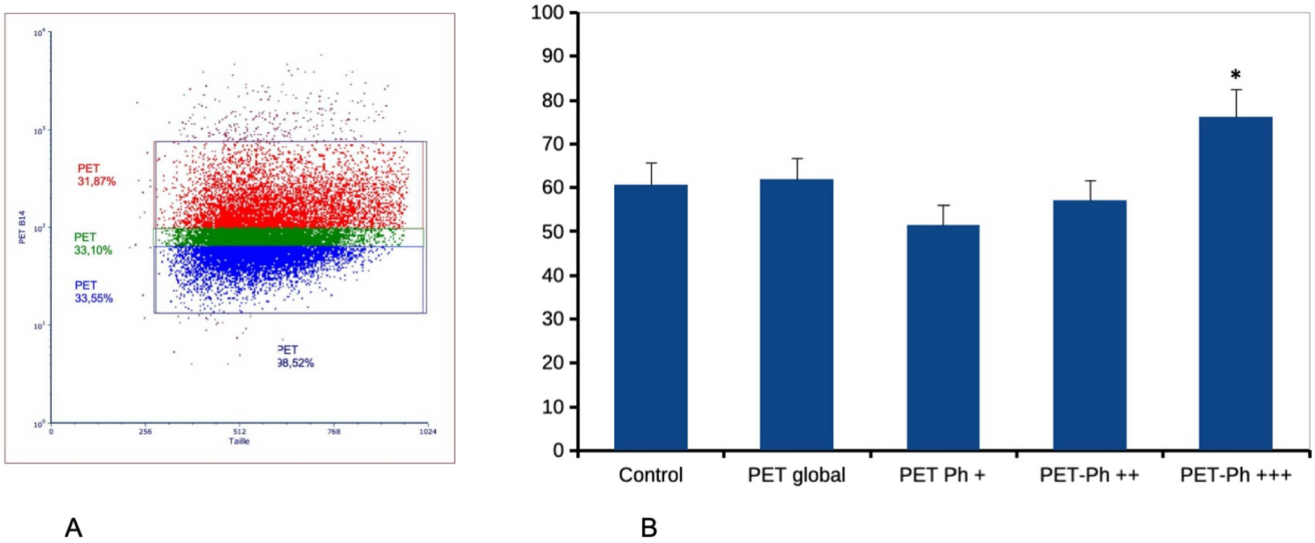

Fig. 5 Phagocytic capacity. Cells were first treated for 24 h with 50 μg ml^{-1} PET particles. After removal of the PET-containing cell culture medium, the cells were treated with green fluorophore-labelled carboxylated polystyrene beads for 3 h. (A) Distribution of the PET-associated fluorescence and of the cell scattering in the flow cytometer. (B) Distribution of the mean fluorescence, indicating the amount of green beads internalized. Results are displayed as mean ± standard deviation (N = 4). The Ph+, Ph++ and Ph+++ populations correspond to the three populations outlined in (A). Significance marks: *$p \leq 0.05$ (Student t-test method, comparison between control and each treatment).

(*e.g.* Mpeg1, increased or Lyz2, decreased) and regulators of cytokine production, such as Lilrb4a, Tnfaip8l2, Tmem43 (all increased in PET-treated cells). This prompted us to investigate the secretion of pro-inflammatory cytokines such as interleukin-6 (IL-6), TNF alpha and the chemokine MCP1, either in response to PET particles alone or in response to PET followed by a bacterial-like challenge (lipopolysaccharide). The results, displayed in Table 1, showed a slight but significant increase in basal TNF production and a decrease in IL-6 production in PET-treated cells challenged with LPS.

Some receptors to danger signals such as TLR2 (increased in PET-treated cells) or collectin 12 (decreased in PET-treated cells) were also found in our proteomic data analysis. This prompted us to check these results by antibody-based assays. We further extended these experiments to surface markers that we had investigated previously in response to PS particles.[35] The results, displayed in Table 2, confirmed the proteomic results.

These data also showed a significant drop in the proportion of collectin 12-positive cells in the PET-treated cells as well as a drop of the surface presence of TLR2 in PET-treated cells, although the total level of intracellular TLR2 increased in PET-treated cells, as predicted by proteomics. We did not observe any significant changes in the polarization markers CD86 and CD204 or in the PD-L1 ligand. However, we observed a decrease in the TLR7 amount in PET-treated cells.

Finally, in order to investigate the dose-dependency of the cellular responses to PET nanoparticles, we treated J7741A.1 cells with 5 μg ml^{-1} PET nanoparticles and investigated the cellular parameters that were significantly impacted at 50 μg ml^{-1}. The results, displayed in Table 3, showed that many of these parameters were not impacted at 5 μg ml^{-1}, except for the lysosomal activity, as measured by the Lysosensor signal, which was increased, as it was at 50 μg ml^{-1}. The TLR7 level also showed a statistical significance, but at such a low ratio level (0.97) that we did not elaborate any further on this parameter. Finally, the oxidative stress was statistically significantly decreased but only slightly at this low PET concentration, while it increased at the 50 μg ml^{-1} concentration.

4. Discussion

The deleterious effects of plastics on life have been widely documented, first on macroplastics (*e.g.* in Derraik *et al.*[4]) but more recently on microplastics[3,19] and nanoplastics.[61,62]

Table 1 Cytokine secretion in response to PET particles

Condition	Value in control cells[a]	Value in PET-treated cells[a]	Ratio	p-Value[b]
IL-6, no LPS	0	0	NA	NA
MCP1 no LPS	10 182 ± 801	9641 ± 225	0.95	0.16
TNF, no LPS	317 ± 41	468 ± 70	1.48	0.0016
IL-6, with LPS[c]	2591 ± 271	1620 ± 131	0.62	8.53×10^{-5}
MCP1, with LPS[c]	91 730 ± 2710	94 527 ± 7548	1.03	0.42
TNF, with LPS[c]	10 135 ± 1012	11 872 ± 1751	1.17	0.07

[a] Values in pg ml^{-1} of medium, expressed as mean ± standard deviation (N = 6). [b] Student t-test. [c] LPS concentration: 1 ng ml^{-1}.

Open Access Article. Published on 01 April 2025. Downloaded on 2/6/2026 8:59:39 AM. This article is licensed under a Creative Commons Attribution-NonCommercial 3.0 Unported Licence.

Table 2 Surface marker expression

Condition	Value in control cells[a]	Value in PET-treated cells[a]	Ratio	p-Value[b]
Collectin 12[c]	158 ± 7	136 ± 12	0.86	0.03
Collectin 12[d]	70 ± 8	48 ± 12	0.69	0.03
CD86	78.5 ± 3.5	81 ± 2	1.03	0.27
CD204	27.3 ± 1.4	28.2 ± 0.7	1.03	0.33
PD-L1	21.8 ± 4.4	24.2 ± 1.1	1.11	0.36
TLR2, total	20.6 ± 1	24.3 ± 0.9	1.18	5.50×10^{-5}
TLR2, surface	41.3 ± 1.3	34.4 ± 4.7	0.83	0.06
TLR7	377 ± 18	306 ± 15	0.81	0.001

[a] Values in arbitrary fluorescence units (mean fluorescence index, MFI), expressed as mean ± standard deviation (N = 4). [b] Student t-test. [c] MFI values for collectin 12-positive cells. [d] Percentage of collectin 12-positive cells in the populations.

Table 3 Parameters measured in response to 5 μg ml^{-1} PET nanoparticles

Condition	Value in control cells[a]	Value in PET-treated cells[a]	Ratio	p-Value[b]
DHR123	3985 ± 127	3518 ± 122	0.88	7×10^{-5}
Lysosensor signal	143 ± 7	225 ± 19	1.57	5×10^{-5}
Collectin 12[c]	19.9 ± 7	20 ± 6	0.86	0.97
Collectin 12[d]	45 ± 17	44 ± 10	0.98	0.98
TLR2, total	18.9 ± 1.4	18.6 ± 0.5	0.98	0.69
TLR7	188 ± 3	183 ± 3	0.97	0.04

[a] Values in arbitrary fluorescence units (mean fluorescence index, MFI), expressed as mean ± standard deviation (N = 4). [b] Student t-test. [c] MFI values for collectin 12-positive cells. [d] Percentage of collectin 12-positive cells in the populations.

It is therefore important to better understand the effects of nanoplastics and microplastics on living cells. Within this general frame, macrophages are a key cell type of interest, as these cells internalize all particulate materials that are either deposited at the surface of the lung alveolae or that have crossed the biological barriers (*e.g.* in Stock *et al.*[29]). Moreover, macrophages are key players in inflammation and in immune responses, and their dysfunction has been linked to either chronic inflammatory diseases in the case of M1-polarized macrophages (*e.g.* in ref. 63) or to cancer growth in the case of M2-polarized macrophages.[64]

It is also particularly interesting to obtain such data on true-to-life plastic particles obtained from consumer products and not from model polymers. Although this will not be the best model for environmentally found particles, which are heavily modified by a myriad of adsorbed chemicals,[65] these true-to-life particles are an excellent model of the particles that are spontaneously released in consumer products.[66] Indeed, as most plastic bottles are made of PET, the true-to-life PET particles used in this work are an excellent model.

As the first step, we investigated the acute toxicity of the PET nanoparticles on macrophages. The toxicity appeared quite low, with a LD20 close to 120 μg ml^{-1}, *i.e.* intermediate between the toxicity of PS particles[67] and the one of PLA particles.[44] We compared the internalization figures for PET particles to those for PS and PLA particles and found that PET particles were more efficiently internalized than the PS and PLA particles that we used for comparison. This may be due to that fact that it is not possible to find control particles that match exactly the physicochemical parameters of the PET NPLs, so that the slightly different size and density for each type of particle may explain these variations, which are however not widely different (66% for PET compared to 45–50% for the other particles). Finally, we tested the effects of endocytosis inhibitors on PET NPL internalization. The inhibitors indicated that part of the internalization is raft-dependent, and part is macropinocytosis-dependent. These data are in accordance with the presence of small particles in the PET NPL population (Fig. 1), which can be internalized by the raft-dependent pathway for articles less than 100 nm in size.[68] It should also be noted that the control experiments carried out with 1 μm PS beads confirm the rather weak specificity of endocytosis inhibitors (*e.g.* nystatin) noted in recent reviews.[68]

For the sake of consistency with our previous experiments on PS and PLA nanoparticles,[44] we decided to investigate the effects of PET nanoparticles at the non-toxic concentration of 50 μg ml^{-1}.

First, and in order to obtain a wide appraisal of the macrophages responses to PET nanoparticles, we used a proteomic screen. Out of 2876 proteins quantified, the proteomic screen highlighted 232 proteins modulated upon treatment with PET, covering several pathways. This proportion of modulated proteins was less important than for PS[34] or PLA[44] nanoparticles. This clearly show that the extent of the cellular responses strongly depends on the nature of the plastics, so that no general rules covering a wide range of plastic particles can be deduced.

 This journal is © The Royal Society of Chemistry 2025

Open Access Article. Published on 01 April 2025. Downloaded on 2/6/2026 8:59:39 AM. This article is licensed under a Creative Commons Attribution-NonCommercial 3.0 Unported Licence.

Indeed, when we instigated the cellular responses through targeted experiments, the conclusions were different for PET particles than for the PS or PLA nanoparticles. First, we determined that endoplasmic reticulum stress is important in the toxicity of the PET particles, in accordance with our proteomic results on proteins such as Retreg1, Ptpn1, Sgpl1, and Canx, which was not the case for PLA nanoparticles, for example.[44]

Second, we did not see any impact on the mitochondrial transmembrane potential. This result was consistent with the one obtained with PLA nanoparticles,[44] and different from the one recently described on PET particles on another macrophage cell line, MH-S.[69]

Third, we did observe a slight increase in the lysosomal activity of the PET-treated cells. As the same response was observed not only with PS and PLA nanoparticles[44] but also for low concentrations of synthetic amorphous silica,[70] we can reasonably infer that this response is consistent with a general response to the phagocytosis of particles.

At this low and not toxic concentration, we did not observe any impact on the phagocytic function of macrophages. In fact, we are quite far from the overload phenomenon,[71,72] which we observed rather at particle concentrations of 500 μg ml^{-1}.[73] This showed, however, that plastic nanoparticles do not have deleterious effects on the phagocytic function of macrophages, which is sometimes not the case for macrophage-toxic nanoparticles such as amorphous silica[46] or zinc oxide.[74]

Regarding the oxidative stress response, we observed a moderate (+14%) but statistically significant response in PET-treated J774A.1 cells. These results were consistent with those obtained on another macrophage cell line, RAW 264.7,[75] but the response was much higher in the MH-S cell line.[69]

These repeated discrepancies between our results and those recently described on the MH-S cell line[69] may find their basis in the different origins of the two cell lines. The MH-S cell line has been produced by *in vitro* immortalization of mouse alveolar macrophages by the SV-40 virus.[76] The J774A.1 cell line used in this study arises from an abdominal cancer induced by the injection of a hydrocarbon[77] and therefore most likely arises from a peritoneal macrophage. These two types of macrophages (peritoneal and alveolar) are known to have a different physiology,[78–80] and it is therefore not surprising that they also show different responses to a stimulus such as PET nanoparticles. This situation may indicate in turn that our results would be more relevant for a plastic contamination after ingestion and translocation through the intestinal barrier[29] than for a respiratory contamination.

Beyond these general responses, we also probed the immune functions of macrophages, such as the production of inflammatory cytokines and the expression of immune-related surface markers. The choice of the markers was guided by our proteomic experiments (*e.g.* collectin 12, TLR2) and by previous experiments carried out with PS nanoparticles (*e.g.* CD86, CD204, TLR7, PD-L1).

Regarding the inflammatory response, the only positive signal that we found was a slight increase (*ca.* 1.5-fold) of basal TNF production in PET-treated cells. Such an increase was close to the one induced by other plastic particles such as PS and PLA,[44] however, lower than the increase induced by synthetic amorphous silica, a known pro-inflammatory particle.[46] Moreover, we did not detect any basal production of interleukin-6 in response to PET particles, a situation that is clearly different from the one induced by synthetic amorphous silica.

Within inflammatory responses, we also probed how the internalization of PET nanoparticles modulated the response to LPS, indicating whether PET internalization may alter the capacity of macrophages to respond to a bacterial infection. Our results (decrease in IL-6 production, increase in TNF production) were similar to those described with PLA and PS nanoparticles,[44] although the changes were of a lesser magnitude with PET particles (*e.g.* 17% increase in TNF production with PET particles instead of 65% increase with PLA and 35% increase with PS).

Regarding the expression of surface markers, we did not find any change in the expression of the macrophage activation marker CD86 or in the expression of the tumor-associated macrophage marker CD 204.[64,81] These results contrasted with those described on the MH-S cell line in response to PET particles,[69] showing once again the difference between the two cell lines.

More significant results were obtained on immune receptors sensing danger signals. As a first example, TL7 showed a moderate (−20%) but significant decrease. TLR7 recognizes single-strand RNA,[82] found in some viruses, and is therefore implicated in antiviral defenses.[82,83] Thus, a decrease in TLR7 expression in response to exposure to PET nanoparticles may induce in turn a decreased ability to fight viral infections at the macrophage level. Regarding TLR2, the situation was even more complex. Proteomics indicated an increase in TLR2 expression, which was confirmed when the total level of TLR2 (intracellular and surface expressed) was probed with antibodies. However, probing the surface expression of TLR2 revealed a decreased presence at the surface (−17%). This is a likely indication that the internalization of PET nanoparticles perturbs the addressing of TLR2 at the cell surface, a phenomenon that the cells counteract by an increased expression of the protein. As TLR2 is normally a cell surface TLR that recognizes various bacterial wall compounds,[84] such a decrease may also indicate a lower ability of PET-treated macrophages to fight bacterial infections.

A decrease was also observed for collectin 12, a surface receptor binding carbohydrate ligands and implied in antitumoral and antibacterial responses.[85,86] Once again, the decrease of this receptor at the surface of PET-treated cells may indicate a lower defense level.

Finally, one of the immune system proteins that shows the highest modulation in PET-treated cells (close to 2.3 reduction) is lysozyme 2, also called lysozyme M in mice.[87]

Open Access Article. Published on 01 April 2025. Downloaded on 2/6/2026 8:59:39 AM. This article is licensed under a Creative Commons Attribution-NonCommercial 3.0 Unported Licence.

Lysozymes are antibacterial proteins conserved in evolution,[88,89] and it has long been shown that they play an important role in the bactericidal activity of macrophages.[90] Moreover, lysozymes play an important role in the modulation of inflammation, as recently reviewed.[91] Quite interestingly, it has long been known that treatment of macrophages with "latex" particles, in fact polystyrene microparticles, reduces both lysozyme production and secretion by macrophages.[92] We detected a decrease in lysozyme production not only in macrophages treated with PS nanoparticles but also in PLA-treated macrophages.[44] However, in both cases the decrease factor was lower, *e.g.* 1.7 in PLA-treated cells, instead of 2.3 for PET-treated cells. Oppositely, lysozyme production is induced in macrophages treated with synthetic amorphous silica,[70] *i.e.* a known pro-inflammatory material with a transient effect.[46,93–95] Thus, owing to the various functions of lysozymes in the integrated immune response,[91] such an important reduction in the production of lysozyme by PET-treated macrophages may perturb the immune functions of PET-treated macrophages, even at a non-toxic concentration.

5. Conclusions

When compared to other plastic particles such as polystyrene or polylactide, PET particles induce less proteome alterations, showing that they induce globally a lesser reaction of macrophages. However, the effects that PET particles show on macrophages are fairly different than those induced by polystyrene or polylactide particles. First, PET particles induce an endoplasmic reticulum stress, which participates in the toxicity of the PET particles. Second and more importantly, PET particles alter the immune functions of macrophages, rather on the side of a decrease of the immune functions. This is illustrated at the cytokinic response to a bacterial-like challenge and at the level of the expression of important proteins in the immune functions of macrophages, such as lysozyme and TLR proteins. Thus, although weakly toxic, PET particles may alter the immune system homeostasis and render organisms more susceptible to infections.

Data availability

The proteomic data have been deposited in the ProteomeXchange Consortium database and are available through the **https://doi.org/10.6019/PXD062730**.

The non proteomic data have been deposited in BioStudies under the **https://doi.org/10.6019/S-BSST1693**.

Author contributions

TR designed and supervised the study. AV, RM, and AH generated and characterized the true-to-life PET nanoplastics. MV performed the viability assays and the experiments with salubrinal. VCF, HD, and SC performed the proteomic experiments, which were then analyzed by TR and ED. VCF performed and interpreted the flow cytometry experiments. TR drafted the initial version of the manuscript, which was completed and amended by all co-authors, who approved the final version of the manuscript.

Conflicts of interest

There are no conflicts of interest to declare.

Acknowledgements

This work used the flow cytometry facility supported by GRAL, a project of the University Grenoble Alpes graduate school (Ecoles Universitaires de Recherche) CBH-EUR-GS (ANR-17-EURE-0003) as well as the platforms of the French Proteomic Infrastructure (ProFI) project (grant ANR-10-INBS-08-03). This work was carried out in the frame of the PlasticHeal project, which has received funding from the European Union's Horizon 2020 research and innovation programme under grant agreement No. 965196. This work was also supported by the ANR Plastox project (grant ANR-21-CE34-0028-04).

References

1 R. Lehner, C. Weder, A. Petri-Fink and B. Rothen-Rutishauser, Emergence of Nanoplastic in the Environment and Possible Impact on Human Health, *Environ. Sci. Technol.*, 2019, **53**, 1748–1765.
2 Y. V. Fan, P. Jiang, R. R. Tan, K. B. Aviso, F. You, X. Zhao, C. T. Lee and J. J. Klemeš, Forecasting plastic waste generation and interventions for environmental hazard mitigation, *J. Hazard. Mater.*, 2022, **424**, 127330.
3 H. S. Charlton-Howard, A. L. Bond, J. Rivers-Auty and J. L. Lavers, 'Plasticosis': Characterising macro- and microplastic-associated fibrosis in seabird tissues, *J. Hazard. Mater.*, 2023, **450**, 131090.
4 J. G. B. Derraik, The pollution of the marine environment by plastic debris: a review, *Mar. Pollut. Bull.*, 2002, **44**, 842–852.
5 K. Enders, R. Lenz, C. A. Stedmon and T. G. Nielsen, Abundance, size and polymer composition of marine microplastics ≥ 10 μm in the Atlantic Ocean and their modelled vertical distribution, *Mar. Pollut. Bull.*, 2015, **100**, 70–81.
6 A. Ter Halle, L. Jeanneau, M. Martignac, E. Jardé, B. Pedrono, L. Brach and J. Gigault, Nanoplastic in the North Atlantic Subtropical Gyre, *Environ. Sci. Technol.*, 2017, **51**, 13689–13697.
7 J. A. Brandon, A. Freibott and L. M. Sala, Patterns of suspended and salp-ingested microplastic debris in the North Pacific investigated with epifluorescence microscopy, *Limnol. Oceanogr. Lett.*, 2020, **5**, 46–53.
8 M. Kedzierski, M. Palazot, L. Soccalingame, M. Falcou-Préfol, G. Gorsky, F. Galgani, S. Bruzaud and M. L. Pedrotti, Chemical composition of microplastics floating on the surface of the Mediterranean Sea, *Mar. Pollut. Bull.*, 2022, **174**, 113284.

 This journal is © The Royal Society of Chemistry 2025

Open Access Article. Published on 01 April 2025. Downloaded on 2/6/2026 8:59:39 AM. This article is licensed under a Creative Commons Attribution-NonCommercial 3.0 Unported Licence.

9 E. S. Jones, S. W. Ross, C. M. Robertson and C. M. Young, Distributions of microplastics and larger anthropogenic debris in Norfolk Canyon, Baltimore Canyon, and the adjacent continental slope (Western North Atlantic Margin, U.S.A.), *Mar. Pollut. Bull.*, 2021, **174**, 113047.

10 L. Cutroneo, M. Capello, A. Domi, S. Consani, P. Lamare, P. Coyle, V. Bertin, D. Dornic, A. Reboa, I. Geneselli and M. Anghinolfi, Microplastics in the abyss: a first investigation into sediments at 2443-m depth (Toulon, France), *Environ. Sci. Pollut. Res.*, 2022, **29**, 9375–9385.

11 T. Mani, A. Hauk, U. Walter and P. Burkhardt-Holm, Microplastics profile along the Rhine River, *Sci. Rep.*, 2015, **5**, 17988.

12 C. Scherer, A. Weber, F. Stock, S. Vurusic, H. Egerci, C. Kochleus, N. Arendt, C. Foeldi, G. Dierkes, M. Wagner, N. Brennholt and G. Reifferscheid, Comparative assessment of microplastics in water and sediment of a large European river, *Sci. Total Environ.*, 2020, **738**, 139866.

13 L. Weiss, W. Ludwig, S. Heussner, M. Canals, J.-F. Ghiglione, C. Estournel, M. Constant and P. Kerhervé, The missing ocean plastic sink: Gone with the rivers, *Science*, 2021, **373**, 107–111.

14 C. J. Weber, C. Opp, J. A. Prume, M. Koch, T. J. Andersen and P. Chifflard, Deposition and in-situ translocation of microplastics in floodplain soils, *Sci. Total Environ.*, 2022, **819**, 152039.

15 H. Golwala, X. Zhang, S. M. Iskander and A. L. Smith, Solid waste: An overlooked source of microplastics to the environment, *Sci. Total Environ.*, 2021, **769**, 144581.

16 A. Chamas, H. Moon, J. Zheng, Y. Qiu, T. Tabassum, J. H. Jang, M. Abu-Omar, S. L. Scott and S. Suh, Degradation Rates of Plastics in the Environment, *ACS Sustainable Chem. Eng.*, 2020, **8**, 3494–3511.

17 L. Lei, M. Liu, Y. Song, S. Lu, J. Hu, C. Cao, B. Xie, H. Shi and D. He, Polystyrene (nano)microplastics cause size-dependent neurotoxicity, oxidative damage and other adverse effects in Caenorhabditis elegans, *Environ. Sci.: Nano*, 2018, **5**, 2009–2020.

18 X. Jiang, Y. Chang, T. Zhang, Y. Qiao, G. Klobučar and M. Li, Toxicological effects of polystyrene microplastics on earthworm (Eisenia fetida), *Environ. Pollut.*, 2020, **259**, 113896.

19 R. Sussarellu, M. Suquet, Y. Thomas, C. Lambert, C. Fabioux, M. E. J. Pernet, N. Le Goïc, V. Quillien, C. Mingant, Y. Epelboin, C. Corporeau, J. Guyomarch, J. Robbens, I. Paul-Pont, P. Soudant and A. Huvet, Oyster reproduction is affected by exposure to polystyrene microplastics, *Proc. Natl. Acad. Sci. U. S. A.*, 2016, **113**, 2430–2435.

20 Y. Song, C. Cao, R. Qiu, J. Hu, M. Liu, S. Lu, H. Shi, K. M. Raley-Susman and D. He, Uptake and adverse effects of polyethylene terephthalate microplastics fibers on terrestrial snails (Achatina fulica) after soil exposure, *Environ. Pollut.*, 2019, **250**, 447–455.

21 A. H. D'Costa, Microplastics in decapod crustaceans: Accumulation, toxicity and impacts, a review, *Sci. Total Environ.*, 2022, **832**, 154963.

22 O. Pikuda, E. Roubeau Dumont, Q. Chen, J.-R. Macairan, S. A. Robinson, D. Berk and N. Tufenkji, Toxicity of microplastics and nanoplastics to Daphnia magna: Current status, knowledge gaps and future directions, *TrAC, Trends Anal. Chem.*, 2023, **167**, 117208.

23 A. Muhammad, X. Zhou, J. He, N. Zhang, X. Shen, C. Sun, B. Yan and Y. Shao, Toxic effects of acute exposure to polystyrene microplastics and nanoplastics on the model insect, silkworm Bombyx mori, *Environ. Pollut.*, 2021, **285**, 117255.

24 M. Alaraby, D. Abass, J. Domenech, A. Hernández and R. Marcos, Hazard assessment of ingested polystyrene nanoplastics in Drosophila larvae, *Environ. Sci.: Nano*, 2022, **9**, 1845–1857.

25 N. R. Brun, P. van Hage, E. R. Hunting, A.-P. G. Haramis, S. C. Vink, M. G. Vijver, M. J. M. Schaaf and C. Tudorache, Polystyrene nanoplastics disrupt glucose metabolism and cortisol levels with a possible link to behavioural changes in larval zebrafish, *Commun. Biol.*, 2019, **2**, 382.

26 I. Brandts, M. Garcia-Ordoñez, L. Tort, M. Teles and N. Roher, Polystyrene nanoplastics accumulate in ZFL cell lysosomes and in zebrafish larvae after acute exposure, inducing a synergistic immune response in vitro without affecting larval survival in vivo, *Environ. Sci.: Nano*, 2020, **7**, 2410–2422.

27 W. Gu, S. Liu, L. Chen, Y. Liu, C. Gu, H. Ren and B. Wu, Single-Cell RNA Sequencing Reveals Size-Dependent Effects of Polystyrene Microplastics on Immune and Secretory Cell Populations from Zebrafish Intestines, *Environ. Sci. Technol.*, 2020, **54**, 3417–3427.

28 L. Li, S. Sun, L. Tan, Y. Wang, L. Wang, Z. Zhang and L. Zhang, Polystyrene Nanoparticles Reduced ROS and Inhibited Ferroptosis by Triggering Lysosome Stress and TFEB Nucleus Translocation in a Size-Dependent Manner, *Nano Lett.*, 2019, **19**, 7781–7792.

29 V. Stock, L. Böhmert, E. Lisicki, R. Block, J. Cara-Carmona, L. K. Pack, R. Selb, D. Lichtenstein, L. Voss, C. J. Henderson, E. Zabinsky, H. Sieg, A. Braeuning and A. Lampen, Uptake and effects of orally ingested polystyrene microplastic particles in vitro and in vivo, *Arch. Toxicol.*, 2019, **93**, 1817–1833.

30 J. Domenech, A. Hernández, L. Rubio, R. Marcos and C. Cortés, Interactions of polystyrene nanoplastics with in vitro models of the human intestinal barrier, *Arch. Toxicol.*, 2020, **94**, 2997–3012.

31 S. Ballesteros, J. Domenech, I. Barguilla, C. Cortés, R. Marcos and A. Hernández, Genotoxic and immunomodulatory effects in human white blood cells after ex vivo exposure to polystyrene nanoplastics, *Environ. Sci.: Nano*, 2020, **7**, 3431–3446.

32 C. Meindl, K. Öhlinger, V. Zrim, T. Steinkogler and E. Fröhlich, Screening for Effects of Inhaled Nanoparticles in Cell Culture Models for Prolonged Exposure, *Nanomaterials*, 2021, **11**, 606.

33 J. Antunes, P. Sobral, M. Martins and V. Branco, Nanoplastics activate a TLR4/p38-mediated pro-inflammatory response in human intestinal and mouse microglia cells, *Environ. Toxicol. Pharm.*, 2023, **104**, 104298.

Open Access Article. Published on 01 April 2025. Downloaded on 2/6/2026 8:59:39 AM. This article is licensed under a Creative Commons Attribution-NonCommercial 3.0 Unported Licence.

34 V. Collin-Faure, B. Dalzon, J. Devcic, H. Diemer, S. Cianférani and T. Rabilloud, Does size matter? A proteomics-informed comparison of the effects of polystyrene beads of different sizes on macrophages, *Environ. Sci.: Nano*, 2022, **9**, 2827–2840.

35 V. Collin-Faure, M. Vitipon, A. Torres, O. Tanyeres, B. Dalzon and T. Rabilloud, The internal dose makes the poison: higher internalization of polystyrene particles induce increased perturbation of macrophages, *Front. Immunol.*, 2023, **14**, 1092743.

36 A. G. Rodríguez-Hernández, J. A. Muñoz-Tabares, J. C. Aguilar-Guzmán and R. Vazquez-Duhalt, A novel and simple method for polyethylene terephthalate (PET) nanoparticle production, *Environ. Sci.: Nano*, 2019, **6**, 2031–2036.

37 A. Villacorta, L. Rubio, M. Alaraby, M. López-Mesas, V. Fuentes-Cebrian, O. H. Moriones, R. Marcos and A. Hernández, A new source of representative secondary PET nanoplastics. Obtention, characterization, and hazard evaluation, *J. Hazard. Mater.*, 2022, **439**, 129593.

38 A. Winkler, F. Fumagalli, C. Cella, D. Gilliland, P. Tremolada and A. Valsesia, Detection and formation mechanisms of secondary nanoplastic released from drinking water bottles, *Water Res.*, 2022, **222**, 118848.

39 J. Zhang, M. Peng, E. Lian, L. Xia, A. G. Asimakopoulos, S. Luo and L. Wang, Identification of Poly(ethylene terephthalate) Nanoplastics in Commercially Bottled Drinking Water Using Surface-Enhanced Raman Spectroscopy, *Environ. Sci. Technol.*, 2023, **57**, 8365–8372.

40 N. Qian, X. Gao, X. Lang, H. Deng, T. M. Bratu, Q. Chen, P. Stapleton, B. Yan and W. Min, Rapid single-particle chemical imaging of nanoplastics by SRS microscopy, *Proc. Natl. Acad. Sci. U. S. A.*, 2024, **121**, e2300582121.

41 B. Prietl, C. Meindl, E. Roblegg, T. R. Pieber, G. Lanzer and E. Fröhlich, Nano-sized and micro-sized polystyrene particles affect phagocyte function, *Cell Biol. Toxicol.*, 2014, **30**, 1–16.

42 V. Paget, S. Dekali, T. Kortulewski, R. Grall, C. Gamez, K. Blazy, O. Aguerre-Chariol, S. Chevillard, A. Braun, P. Rat and G. Lacroix, Specific Uptake and Genotoxicity Induced by Polystyrene Nanobeads with Distinct Surface Chemistry on Human Lung Epithelial Cells and Macrophages, *PLoS One*, 2015, **10**, e0123297.

43 I. Florance, S. Ramasubbu, A. Mukherjee and N. Chandrasekaran, Polystyrene nanoplastics dysregulate lipid metabolism in murine macrophages in vitro, *Toxicology*, 2021, **458**, 152850.

44 V. Collin-Faure, M. Vitipon, H. Diemer, S. Cianferani, E. Darrouzet and T. Rabilloud, Biobased, Biodegradable but not bio-neutral: about the effects of polylactic acid nanoparticles on macrophages, *Environ. Sci.: Nano*, 2024, **11**, 4102–4116.

45 T. Behnke, C. Würth, K. Hoffmann, M. Hübner, U. Panne and U. Resch-Genger, Encapsulation of Hydrophobic Dyes in Polystyrene Micro- and Nanoparticles via Swelling Procedures, *J. Fluoresc.*, 2011, **21**, 937–944.

46 A. Torres, V. Collin-Faure, D. Fenel, J.-A. Sergent and T. Rabilloud, About the Transient Effects of Synthetic Amorphous Silica: An In Vitro Study on Macrophages, *Int. J. Mol. Sci.*, 2022, **24**, 220.

47 S. Gimondi, J. Vieira De Castro, R. L. Reis, H. Ferreira and N. M. Neves, On the size-dependent internalization of sub-hundred polymeric nanoparticles, *Colloids Surf., B*, 2023, **225**, 113245.

48 A. von Delwig, E. Bailey, D. M. Gibbs and J. H. Robinson, The route of bacterial uptake by macrophages influences the repertoire of epitopes presented to CD4 T cells, *Eur. J. Immunol.*, 2002, **32**, 3714–3719.

49 S. B. Horwitz, G. H. Chia, C. Harracksingh, S. Orlow, S. Pifko-Hirst, J. Schneck, L. Sorbara, M. Speaker, E. W. Wilk and O. M. Rosen, Trifluoperazine inhibits phagocytosis in a macrophagelike cultured cell line, *J. Cell Biol.*, 1981, **91**, 798–802.

50 L. Muller, L. Fornecker, M. Chion, A. Van Dorsselaer, S. Cianférani, T. Rabilloud and C. Carapito, Extended investigation of tube-gel sample preparation: a versatile and simple choice for high throughput quantitative proteomics, *Sci. Rep.*, 2018, **8**, 8260.

51 C. Cavazza, V. Collin-Faure, J. Pérard, H. Diemer, S. Cianférani, T. Rabilloud and E. Darrouzet, Proteomic analysis of Rhodospirillum rubrum after carbon monoxide exposure reveals an important effect on metallic cofactor biosynthesis, *J. Proteomics*, 2022, **250**, 104389.

52 T. Lyubimova, S. Caglio, C. Gelfi, P. G. Righetti and T. Rabilloud, Photopolymerization of polyacrylamide gels with methylene blue, *Electrophoresis*, 1993, **14**, 40–50.

53 O. Hammer, D. A. T. Harper and P. D. Ryan, Paleontological statistics software package for education and data analysis, *Palaeontol. Electronica*, 2001, **4**, 9.

54 D. W. Huang, B. T. Sherman and R. A. Lempicki, Bioinformatics enrichment tools: paths toward the comprehensive functional analysis of large gene lists, *Nucleic Acids Res.*, 2009, **37**, 1–13.

55 S. W. Perry, J. P. Norman, J. Barbieri, E. B. Brown and H. A. Gelbard, Mitochondrial membrane potential probes and the proton gradient: a practical usage guide, *BioTechniques*, 2011, **50**, 98–115.

56 J. F. Keij, C. Bell-Prince and J. A. Steinkamp, Staining of mitochondrial membranes with 10-nonyl acridine orange, MitoFluor Green, and MitoTracker Green is affected by mitochondrial membrane potential altering drugs, *Cytometry*, 2000, **39**, 203–210.

57 G. Abel, J. Szollosi and J. Fachet, Phagocytosis of fluorescent latex microbeads by peritoneal macrophages in different strains of mice: a flow cytometric study, *Eur. J. Immunogenet.*, 1991, **18**, 239–245.

58 K. R. Clarke, Non-parametric multivariate analyses of changes in community structure, *Aust. J. Ecol.*, 1993, **18**, 117–143.

59 M. Boyce, K. F. Bryant, C. Jousse, K. Long, H. P. Harding, D. Scheuner, R. J. Kaufman, D. Ma, D. M. Coen, D. Ron and J. Yuan, A selective inhibitor of eIF2alpha dephosphorylation protects cells from ER stress, *Science*, 2005, **307**, 935–939.

60 T. L. Pan, P. W. Wang, Y. C. Hung, C. H. Huang and K. M. Rau, Proteomic analysis reveals tanshinone IIA enhances apoptosis of advanced cervix carcinoma CaSki cells through

 This journal is © The Royal Society of Chemistry 2025

Open Access Article. Published on 01 April 2025. Downloaded on 2/6/2026 8:59:39 AM. This article is licensed under a Creative Commons Attribution-NonCommercial 3.0 Unported Licence.

mitochondria intrinsic and endoplasmic reticulum stress pathways, *Proteomics*, 2013, **13**, 3411–3423.

61 R. Shen, K. Yang, X. Cheng, C. Guo, X. Xing, H. Sun, D. Liu, X. Liu and D. Wang, Accumulation of polystyrene microplastics induces liver fibrosis by activating cGAS/STING pathway, *Environ. Pollut.*, 2022, **300**, 118986.

62 R. Marfella, F. Prattichizzo, C. Sardu, G. Fulgenzi, L. Graciotti, T. Spadoni, N. D'Onofrio, L. Scisciola, R. La Grotta, C. Frigé, V. Pellegrini, M. Municinò, M. Siniscalchi, F. Spinetti, G. Vigliotti, C. Vecchione, A. Carrizzo, G. Accarino, A. Squillante, G. Spaziano, D. Mirra, R. Esposito, S. Altieri, G. Falco, A. Fenti, S. Galoppo, S. Canzano, F. C. Sasso, G. Matacchione, F. Olivieri, F. Ferraraccio, I. Panarese, P. Paolisso, E. Barbato, C. Lubritto, M. L. Balestrieri, C. Mauro, A. E. Caballero, S. Rajagopalan, A. Ceriello, B. D'Agostino, P. Iovino and G. Paolisso, Microplastics and Nanoplastics in Atheromas and Cardiovascular Events, *N. Engl. J. Med.*, 2024, **390**, 900–910.

63 R. F. Hamilton, S. A. Thakur and A. Holian, Silica binding and toxicity in alveolar macrophages, *Free Radicals Biol. Med.*, 2008, **44**, 1246–1258.

64 J. Song, T. Xiao, M. Li and Q. Jia, Tumor-associated macrophages: Potential therapeutic targets and diagnostic markers in cancer, *Pathol., Res. Pract.*, 2023, **249**, 154739.

65 F. G. Torres, D. C. Dioses-Salinas, C. I. Pizarro-Ortega and G. E. De-la-Torre, Sorption of chemical contaminants on degradable and non-degradable microplastics: Recent progress and research trends, *Sci. Total Environ.*, 2021, **757**, 143875.

66 Y. Huang, K. K. Wong, W. Li, H. Zhao, T. Wang, S. Stanescu, S. Boult, B. van Dongen, P. Mativenga and L. Li, Characteristics of nano-plastics in bottled drinking water, *J. Hazard. Mater.*, 2022, **424**, 127404.

67 V. Olivier, J. L. Duval, M. Hindié, P. Pouletaut and M. D. Nagel, Comparative particle-induced cytotoxicity toward macrophages and fibroblasts, *Cell Biol. Toxicol.*, 2003, **19**, 145–159.

68 J. J. Rennick, A. P. R. Johnston and R. G. Parton, Key principles and methods for studying the endocytosis of biological and nanoparticle therapeutics, *Nat. Nanotechnol.*, 2021, **16**, 266–276.

69 A. Tavakolpournegari, A. Villacorta, M. Morataya-Reyes, J. Arribas Arranz, G. Banaei, S. Pastor, A. Velázquez, R. Marcos, A. Hernández and B. Annangi, Harmful effects of true-to-life nanoplastics derived from PET water bottles in human alveolar macrophages, *Environ. Pollut.*, 2024, **348**, 123823.

70 A. Torres, V. Collin-Faure, H. Diemer, C. Moriscot, D. Fenel, B. Gallet, S. Cianférani, J.-A. Sergent and T. Rabilloud, Repeated Exposure of Macrophages to Synthetic Amorphous Silica Induces Adaptive Proteome Changes and a Moderate Cell Activation, *Nanomaterials*, 2022, **12**, 1424.

71 C. L. Tran, A. D. Jones and K. Donaldson, Evidence of overload, dissolution and breakage of MMVF10 fibres in the RCC chronic inhalation study, *Exp. Toxicol. Pathol.*, 1996, **48**, 500–504.

72 D. B. Warheit, J. F. Hansen, I. S. Yuen, D. P. Kelly, S. I. Snajdr and M. A. Hartsky, Inhalation of high concentrations of low toxicity dusts in rats results in impaired pulmonary clearance mechanisms and persistent inflammation, *Toxicol. Appl. Pharmacol.*, 1997, **145**, 10–22.

73 J. Devcic, M. Dussol, V. Collin-Faure, J. Pérard, D. Fenel, G. Schoehn, M. Carrière, T. Rabilloud and B. Dalzon, Immediate and Sustained Effects of Cobalt and Zinc-Containing Pigments on Macrophages, *Front. Immunol.*, 2022, **13**, 865239.

74 C. Aude-Garcia, B. Dalzon, J. L. Ravanat, V. Collin-Faure, H. Diemer, J. M. Strub, S. Cianferani, A. Van Dorsselaer, M. Carriere and T. Rabilloud, A combined proteomic and targeted analysis unravels new toxic mechanisms for zinc oxide nanoparticles in macrophages, *J. Proteomics*, 2016, **134**, 174–185.

75 J. C. Aguilar-Guzmán, K. Bejtka, M. Fontana, E. Valsami-Jones, A. M. Villezcas, R. Vazquez-Duhalt and A. G. Rodríguez-Hernández, Polyethylene terephthalate nanoparticles effect on RAW 264.7 macrophage cells, *Microplast. Nanoplast.*, 2022, **2**, 9.

76 I. N. Mbawuike and H. B. Herscowitz, MH-S, a murine alveolar macrophage cell line: morphological, cytochemical, and functional characteristics, *J. Leukocyte Biol.*, 1989, **46**, 119–127.

77 P. Ralph, J. Prichard and M. Cohn, Reticulum cell sarcoma: an effector cell in antibody-dependent cell-mediated immunity, *J. Immunol.*, 1975, **114**, 898–905.

78 A. M. Guth, W. J. Janssen, C. M. Bosio, E. C. Crouch, P. M. Henson and S. W. Dow, Lung environment determines unique phenotype of alveolar macrophages, *Am. J. Physiol.*, 2009, **296**, L936–L946.

79 C. C. Bain and A. S. MacDonald, The impact of the lung environment on macrophage development, activation and function: diversity in the face of adversity, *Mucosal Immunol.*, 2022, **15**, 223–234.

80 G. A. Heieis, T. A. Patente, L. Almeida, F. Vrieling, T. Tak, G. Perona-Wright, R. M. Maizels, R. Stienstra and B. Everts, Metabolic heterogeneity of tissue-resident macrophages in homeostasis and during helminth infection, *Nat. Commun.*, 2023, **14**, 5627.

81 J. Gudgeon, J. L. Marín-Rubio and M. Trost, The role of macrophage scavenger receptor 1 (MSR1) in inflammatory disorders and cancer, *Front. Immunol.*, 2022, **13**, 1012002.

82 S. S. Diebold, T. Kaisho, H. Hemmi, S. Akira and C. Reis e Sousa, Innate antiviral responses by means of TLR7-mediated recognition of single-stranded RNA, *Science*, 2004, **303**, 1529–1531.

83 Z. Zhang, U. Ohto and T. Shimizu, Toward a structural understanding of nucleic acid-sensing Toll-like receptors in the innate immune system, *FEBS Lett.*, 2017, **591**, 3167–3181.

84 T. Kawai, M. Ikegawa, D. Ori and S. Akira, Decoding Toll-like receptors: Recent insights and perspectives in innate immunity, *Immunity*, 2024, **57**, 649–673.

85 K. Nakamura, H. Funakoshi, K. Miyamoto, F. Tokunaga and T. Nakamura, Molecular cloning and functional characterization of a human scavenger receptor with C-type

Open Access Article. Published on 01 April 2025. Downloaded on 2/6/2026 8:59:39 AM.
This article is licensed under a Creative Commons Attribution-NonCommercial 3.0 Unported Licence.

lectin (SRCL), a novel member of a scavenger receptor family, *Biochem. Biophys. Res. Commun.*, 2001, **280**, 1028–1035.

86 T. Yoshida, Y. Tsuruta, M. Iwasaki, S. Yamane, T. Ochi and R. Suzuki, SRCL/CL-P1 recognizes GalNAc and a carcinoma-associated antigen, Tn antigen, *J. Biochem.*, 2003, **133**, 271–277.

87 M. Cross, I. Mangelsdorf, A. Wedel and R. Renkawitz, Mouse lysozyme M gene: isolation, characterization, and expression studies, *Proc. Natl. Acad. Sci. U. S. A.*, 1988, **85**, 6232–6236.

88 R. K. Pipe, Hydrolytic enzymes associated with the granular haemocytes of the marine mussel Mytilus edulis, *Histochem. J.*, 1990, **22**, 595–603.

89 L. Callewaert and C. W. Michiels, Lysozymes in the animal kingdom, *J. Biosci.*, 2010, **35**, 127–160.

90 W. D. Biggar and J. M. Sturgess, Role of lysozyme in the microbicidal activity of rat alveolar macrophages, *Infect. Immun.*, 1977, **16**, 974–982.

91 S. A. Ragland and A. K. Criss, From bacterial killing to immune modulation: Recent insights into the functions of lysozyme, *PLoS Pathog.*, 2017, **13**, e1006512.

92 S. Gordon, J. Todd and Z. A. Cohn, In vitro synthesis and secretion of lysozyme by mononuclear phagocytes, *J. Exp. Med.*, 1974, **139**, 1228–1248.

93 D. B. Warheit, T. A. McHugh and M. A. Hartsky, Differential pulmonary responses in rats inhaling crystalline, colloidal or amorphous silica dusts, *Scand. J. Work, Environ. Health*, 1995, **21**(Suppl 2), 19–21.

94 C. J. Johnston, K. E. Driscoll, J. N. Finkelstein, R. Baggs, M. A. O'Reilly, J. Carter, R. Gelein and G. Oberdorster, Pulmonary chemokine and mutagenic responses in rats after subchronic inhalation of amorphous and crystalline silica, *Toxicol. Sci.*, 2000, **56**, 405–413.

95 C. M. Sayes, K. L. Reed and D. B. Warheit, Assessing toxicity of fine and nanoparticles: comparing in vitro measurements to in vivo pulmonary toxicity profiles, *Toxicol. Sci.*, 2007, **97**, 163–180.

This journal is © The Royal Society of Chemistry 2025